# The chemical bond and s-d hybridization in coinage metal(I) cyanides

Matteo De Santis,[†] Sergio Rampino,[‡,§] Loriano Storchi,[*,¶,‡] Leonardo Belpassi,[*,‡] and Francesco Tarantelli[†,‡]

[†]*Dipartimento di Chimica, Biologia e Biotecnologie, Università degli Studi di Perugia, Via Elce di Sotto 8, 06123 Perugia, Italy*

[‡]*Istituto di Scienze e Tecnologie Molecolari, Consiglio Nazionale delle Ricerche c/o Dipartimento di Chimica, Biologia e Biotecnologie, Università degli Studi di Perugia, Via Elce di Sotto 8, 06123 Perugia, Italy*

[¶]*Dipartimento di Farmacia, Università degli Studi 'G. D'Annunzio', Via dei Vestini 31, 66100 Chieti, Italy*

[§]*Present address: Scuola Normale Superiore, Piazza dei Cavalieri 7, 56126 Pisa (Italy)*

E-mail: loriano@storchi.org; belp@thch.unipg.it

**Abstract**

We present a four-component relativistic density functional theory study of the chemical bond and s-d hybridization in the group-11 cyanides M–CN (M = Cu, Ag, Au). The analysis is carried out within the charge-displacement/natural orbital for chemical valence (CD-NOCV) scheme, which allows us to single out meaningful contributions to the total charge rearrangement that arises upon bond formation and to quantify the components of the Dewar-Chatt-Duncanson bonding model (the ligand-to-metal donation and metal-to-ligand back-donation). The M-CN bond is characterized by a large donation from the cyanide ion to the metal cation and by two small back-donation components from the metal towards the cyanide anion. The case of gold cyanide elucidates the peculiar role of the relativistic effects in determining the characteristics of the Au–C bond with respect to the copper and silver homologues. In AuCN, the donation and back-donation components are significantly enhanced and the spin-orbit coupling, removing the degeneracy of the $5d$ atomic orbitals, induces a substantial split in the back-donation components.

A simple spatial analysis of the NOCV-pair density, related to the ligand-to-metal donation component, allows us to quantify, with unprecedented accuracy, the charge rearrangement due to the s-d hybridization occurring at the metal site. The s-d hybridization plays a key role in determining the shape and size of the metal: it removes electron density from the bond axis and induces a significant flattening at the metal site in trans position to the ligand. The s-d hybridization is present in all noble metal complexes, influencing the bond distances, and its effect is enhanced for Au, which is consistent with the preference of gold to form linear complexes. A comparative investigation of simple complexes $[AuL]^{+/0}$ of $Au^+$ with different ligands (L=$F^-$, N-Heterocyclic Carbene, CO, $PH_3$) shows that the s-d hybridization mechanism is also influenced by the nature of the ligand.

# Introduction

The current great interest in the photophysics, photochemistry and catalytic activity of $d^{10}$ complexes of the coinage metals is fully attested in the literature.[1–5] Gold in particular plays an important role in scientific and technological areas ranging from catalysis, medical and pharmacological research to optoelectronics.[6–9] It is well known that the electronic structure and properties of gold are strongly influenced by relativity. In particular, the relativistic 6s-contraction/stabilization results in an increase of both the first ionization potential and electron affinity, which, combined with the (indirect) relativistic expansion/destabilization of the 5d shell leads to a substantial decrease of the d/s gap. Thus, in spite of its proverbial nobleness, gold has a rich chemistry and exhibits a stronger tendency to form bonds with covalent/multiple bond character than lighter homologues.[10,11] In nanotechnology, for instance, the strong tendency of gold to form covalent bonds is at the core of the ligand-protected gold nanoparticles[12,13] and the strong 5d/6s orbitals hybridization has been suggested to be the origin of the larger propensity of gold to form planar structure clusters than other coinage metals.[14] Also, the nature of the Au-C bond is at the core of homogeneous and heterogeneous gold catalysis,[15–17] making cationic gold(I) complexes especially versatile catalysts. They can act as strong Lewis acids, with a significant back-donation ability[18,19] that, modulated by the electronic properties of the ancillary ligand,[20] provides great efficiency in a growing number of chemical transformations, including the selective activation of alkynes.[21,22]

The tendency of gold to form covalent bonds is even more eye-catching when we consider its surprising ability to stabilize compounds with noble gases.[23–25] For instance, the $AuXe^+$ and $XeAuXe^+$ molecules have been observed in mass spectroscopy by Schwarz et al.[26] in 1998 and $[AuXe_4^{2+}]$ in bulk[27] by Seidel and Seppelt since 2000. Simple halides of Au(I) are known to form stable compounds with the noble gases (NgAuX (Ng=Ne, Ar, Kr; X=Cl, F))[28] with a significant charge-transfer contribution from the noble gas to Au, which stabilizes the noble-gas/noble-metal interaction.[29] A similar mechanism has been proposed to rationalize the experimental evidence of exceptionally strong Au-Ar bonds in Ar complexes of mixed

Au-Ag trimers.[30] High level ab-initio calculations show that Au and Cu have a surprisingly high interaction energy with He in the HeAuF and HeCuF complexes, twice that of Ne-Au in NeAuF, with an unexpected back-donation component from the metal to He found to stabilize these systems.[31]

Experimental and theoretical studies on simple homologous species of group 11 metals (Cu, Ag, Au) have highlighted the specific role of relativistic effects and the peculiar bonding features of gold.[32] Of particular interest are the simple coinage metal cyanides M(CN), with M=Cu, Ag and Au. For instance, Au(CN) is the basic unit of the $Au(CN)_2^-$ ion, which is overall the most important species involved in gold production. Furthermore, gold(I) cyanide polymer assemblies in the solid phase act as frustrated magnets[33] and the formation of gold trimer complexes, $[Au(CN)_2]_3$, has been directly observed in solution with femtosecond X-ray scattering.[34] The bond in dicyanoaurate oligomers has been actively investigated in order to shed light on their spectroscopic and excited-state properties[35–37] and, in order to reproduce the experimental data, consideration of the spin-orbit coupling is found to be essential. Photoelectron experiments on $Au(CN)_2^-$, by comparison with its lighter congeners, $Ag(CN)_2^-$ and $Cu(CN)_2^-$, hint at a significant covalent character of the Au-C bond.[38,39] The atomic-like transitions in $Cu(CN)_2^-$ are indeed consistent with a more ionic bond nature whereas the bond in $Ag(CN)_2^-$ is expected to be of intermediate character. The authors point out that the high stability of $Au(CN)_2^-$ is consistent with the covalent character of the bond and surmise that s-d hybridization enhances gold ability to form multiple bonds, which would explain the short Au-C bond distance in this system.[38,39] A number of high-precision calculations already exist for the cyanides of noble metals (see Refs.[40,41] and references therein). Frenking et al.(2003) investigated the metal-C bonds[42] in cyanides and isocyanides of coinage metals ($[M(CN)_2^-]$, with M=Cu, Ag, Au), analyzing the chemical bond in terms of a well-defined energy partition scheme. They pointed out that covalency between Au and CN is more important than between Cu, or Ag, and CN. The contribution of the metal-to-ligand back-donation (multiple bond character) was estimated to be negligible. A qualitative

bonding analysis by Pyykkö et al.,[40] based on on the inspection of the molecular orbitals and in consideration of the short M-C bond distance (just few pm longer than those predicted for triple-bond covalent radii), suggested a multiple character of the Au-C bond. A similar conclusion has been drawn by Ruud et al.[41] in the case of AuCN. In photoelectron imaging experiments, Fan et al.[43] found that the electron affinities of CuCN and AgCN are larger than those of the metal atoms, while for AuCN it is smaller. The authors suggested a transition from more ionic to more covalent bonding as one goes from CuCN to AuCN and attributed the increased covalent character in AuCN mainly to $\sigma$ donation, which is expected to be stronger in the Au case than for the other coinage metals. The short Au-C bond has been preferably ascribed to the significant s-d hybridization mechanism, which is expected to reduce the repulsive force between the Au d shell and the ligand electrons, rather than to a multiple bond character of the Au-C bond.

In this paper we tackle the study of the chemical bond in coinage-metal cyanides by means of the so-called charge-displacement (CD) via natural orbital for chemical valence scheme (CD-NOCV).[44] In particular we apply a recent implementation that extend the applicability of the method to the fully relativistic four-component framework. In this way, we are able to give a reliable quantitative measure of the donation and back-donation constituents of the bond, and thus to assess the extent of its multiple character with the most accurate inclusion of relativistic effects and spin-orbit coupling. Furthermore, a detailed analysis of the spatial extent of NOCV spinors allows us to disentangle for the first time the ligand-to-metal donation component from the charge rearrangement due to s-d hybridization. Thus we quantify s-d hybridization in the coinage-metal cyanides and how it is influenced by relativity. We also demonstrate that the s-d hybridization mechanism, causing a decrease of electron density along the bond axis, induces a flattening at the metal site, with a significant effect on bond distances in $d^{10}$ complexes. A comparative investigation on some simple complexes $[AuL]^{+/0}$ of $Au^+$ bearing different ligands (L=$F^-$, N-Heterocyclic Carbene, CO, $PH_3$) shows that a such mechanism is general and can be quantitatively influenced by the nature of the

ligand.

# Results and Discussion

## Bonding in CuCN, AgCN and AuCN: NOCV-CD analysis

In the present section we aim to characterize the metal-carbon bond in the series of the M(CN) complexes with M = Cu, Ag and Au. In particular, we provide a quantitative assessment of the Dewar-Chat-Duncanson (DCD) bonding constituents (ligand-to-metal donation and metal-to-ligand backdonation) and how these are tuned by the relativistic effects, which become increasingly important going down the periodic table. We base our analysis on the CD-NOCV methodology, recently extended to the fully relativistic four-component framework (see the section on Methods and Computational Details) and implemented in the code BERTHA.

We begin by mentioning that our calculations give energies of dissociation of the complexes into $M^+$ and $CN^-$ of 204.4, 178.2, 224.5 kcal/mol for M=Cu, Ag, Au, respectively. This reproduces the typical "V" shape pattern which has been previously observed for these systems.[42]

The results of our CD-NOCV analysis are reported in Figures 1, 2 and 3 where $\Delta\rho$, $\Delta\rho'$ (including their difference, $\Delta\rho^{\text{anti}}$) and the most significant NOCV-pairs density decomposition ($\Delta\rho'_k$, with $k = 1, 2, 3, 4$) are shown as isosurface plots together with the distinct NOCV densities ($|\Phi_{+k}|^2$, $|\Phi_{-k}|^2$ with $k = 1, 2, 3, 4$). The related CD functions are reported in Figure 4, the charge transfer (CT) values extracted from these CD functions are summarized for all the systems in Table 1. In the table, the NOCV eigenvalues are also reported.

All systems have their molecular axis along the $z$ axis and the coinage metal position is set at the origin of the reference frame. As expected, the data show that upon bond formation between the fragments $M^+$ and $CN^-$, a significant charge rearrangement takes place. All coinage metal cations present a charge density accumulation (blue isosurface), while a clear

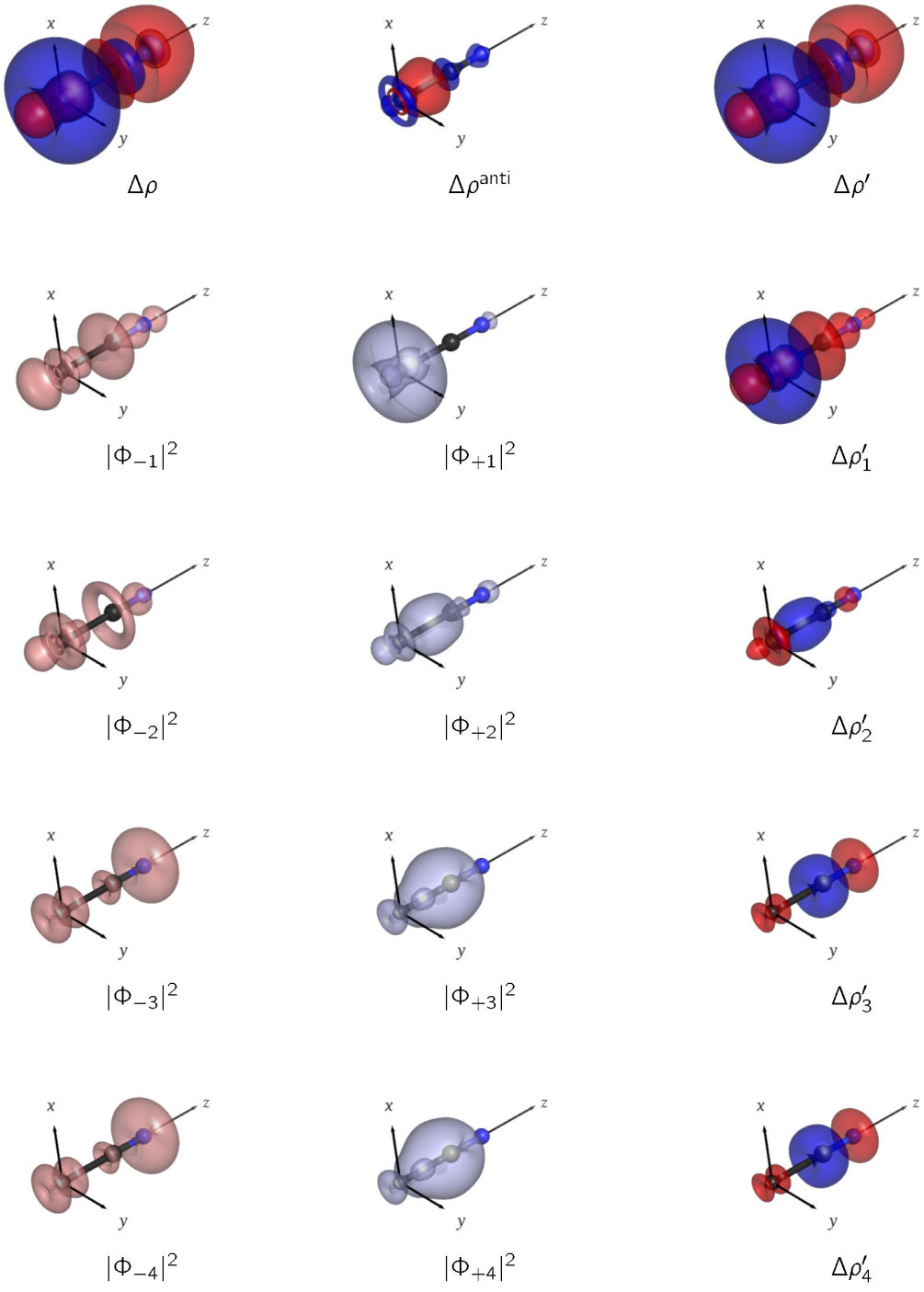


Figure 1: On top $\Delta\rho$, $\Delta\rho^{\text{anti}}$, $\Delta\rho'$ and the $\Delta\rho'_k$ components on the right side are depicted as isodensity surfaces ($\pm 0.0014$ a.u) for CuCN. NOCV-pairs $\left\{|\Phi_{-k}|^2, |\Phi_{+k}|^2\right\}$ are also shown by means of isodensity surfaces ($\pm 0.005$ a.u).

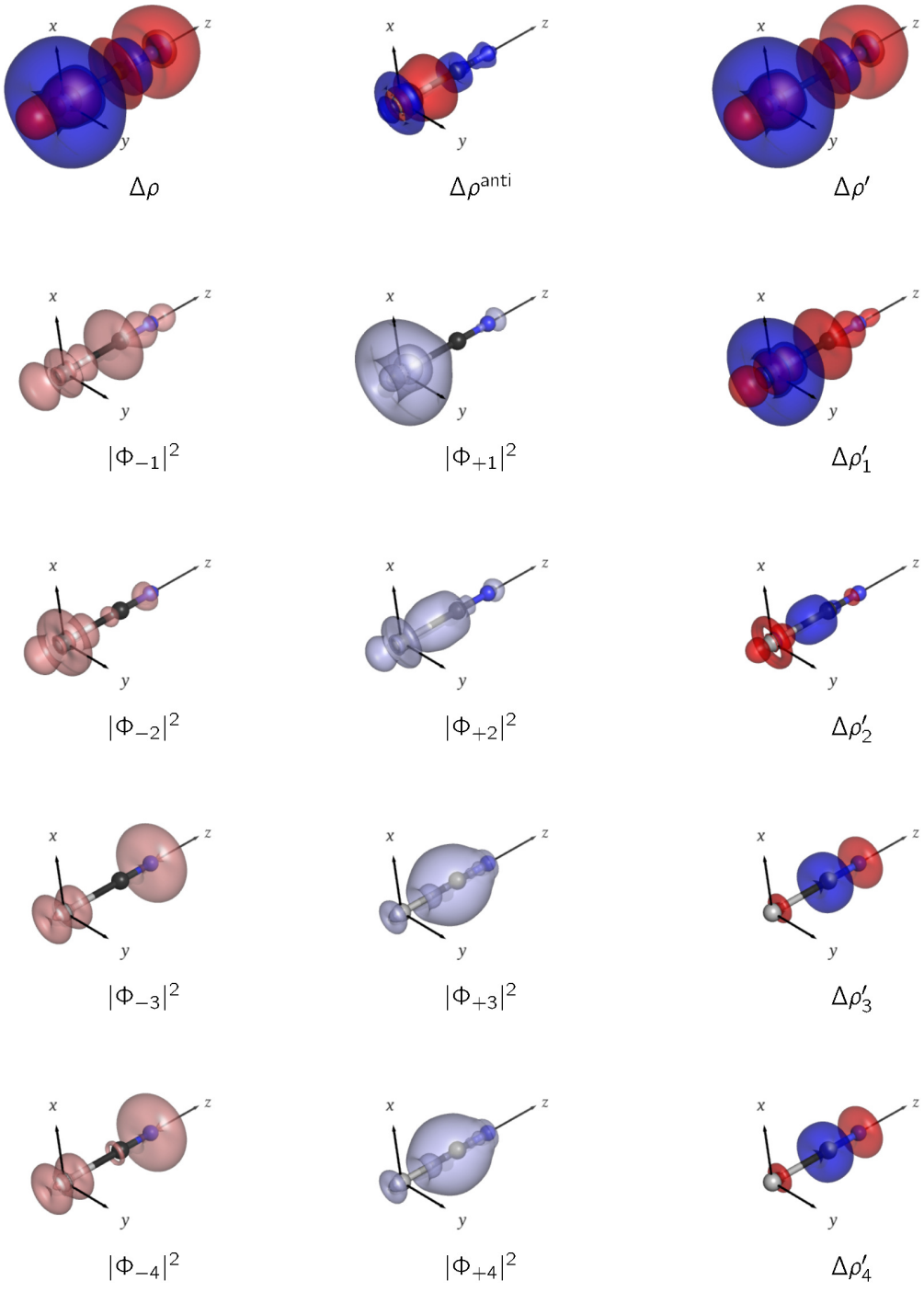


Figure 2: On top $\Delta\rho$, $\Delta\rho^{\text{anti}}$, $\Delta\rho'$ and the $\Delta\rho'_k$ components on the right side are depicted as isodensity surfaces ($\pm 0.0014$ a.u) for AgCN. NOCV-pairs $\left\{|\Phi_{-k}|^2, |\Phi_{+k}|^2\right\}$ are also shown by means of isodensity surfaces ($\pm 0.005$ a.u).

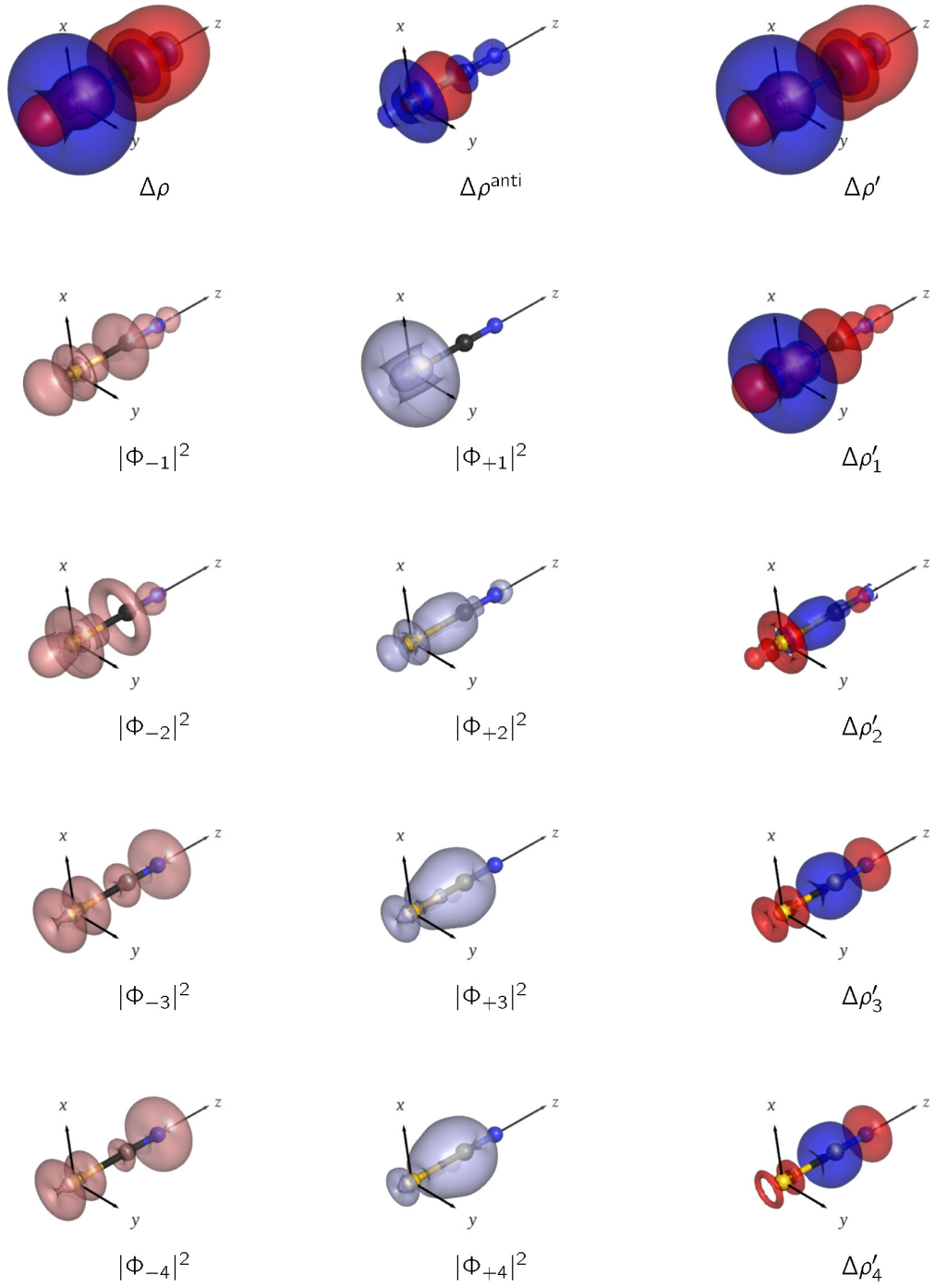


Figure 3: On top $\Delta\rho$, $\Delta\rho^{\text{anti}}$, $\Delta\rho'$ and the $\Delta\rho'_k$ components on the right side are depicted as isodensity surfaces ($\pm 0.0014$ a.u) for AuCN. NOCV-pairs $\left\{|\Phi_{-k}|^2, |\Phi_{+k}|^2\right\}$ are also shown by means of isodensity surfaces ($\pm 0.005$ a.u).

Table 1: Eigenvalues ($v_k$) and charge transfer (CT) corresponding to NOCVs for CuCN, AgCN and AuCN. The first two entry of the table refer to $\Delta\rho$ and $\Delta\rho^{'}$ (see the Methodology section for details).

| | CuCN | | AgCN | | AuCN | |
|---|---|---|---|---|---|---|
| | $v_k$ | CT/$e$ | $v_k$ | CT/$e$ | $v_k$ | CT/$e$ |
| $\Delta\rho$ | - | 0.275 | - | 0.297 | - | 0.400 |
| $\Delta\rho'$ | - | 0.275 | - | 0.304 | - | 0.395 |
| $\Delta\rho'_1$ | 0.680 | 0.322 | 0.623 | 0.345 | 0.965 | 0.484 |
| $\Delta\rho'_2$ | 0.278 | -0.029 | 0.220 | -0.036 | 0.312 | -0.034 |
| $\Delta\rho'_3$ | 0.218 | -0.015 | 0.191 | -0.003 | 0.264 | -0.041 |
| $\Delta\rho'_4$ | 0.217 | -0.013 | 0.191 | -0.007 | 0.254 | -0.017 |

charge depletion occurs at the $CN^-$ site (red isosurface). Closer inspection shows that the overall charge rearrangement at the metal site, of roughly toroidal shape, occurs not only towards the internuclear region but also in the region surrounding the metal itself. This can be clearly interpreted as the partial filling of formally empty $s$-type orbitals of the $nd^{10}$ cations. Interestingly, all metals are also characterized, at their left side (in trans position to the $CN^-$ moiety), by a narrow zone of electron density depletion (red lobe at the metal site). Hence, as we shall discuss in more detail later, the electron density rearrangement at the cation has a complex, far from obvious, pattern. As stated above, we also show $\Delta\rho^{anti}$ for all systems, which is the density rearrangement occurring upon going from the separate A and B fragments to the promolecule (antisymmetrized non-interacting system, see the Methodology section). As has been discussed by Mitoraj et al.[45], this contribution removes the orbital overlap between the two fragments, shifting charge density from the inter-fragments region towards the fragments. The $\Delta\rho^{\text{anti}}$ contour plot thus exhibits a red lobe, denoting charge depletion, extending over the inter-fragment region. Although this is not negligible, it has a marginal effect on the overall bonding picture we present, and indeed, as can be seen, $\Delta\rho$ and $\Delta\rho'$ are very similar.

By means of the NOCVs analysis the most important contributions to the overall electron density rearrangement ($\Delta\rho'$) can be now singled out and thus the distinct DCD components can be qualitatively recognized by simple inspection of the NOCV-pair densities, $\Delta\rho'_k$. These

components can then be quantified by an analysis of the associated CD functions, as discussed below. The NOCV-pair density $\Delta\rho'_1$ is the main contribution to $\Delta\rho'$ (corresponding to the largest eigenvalue, $v_1$) and clearly makes up the ligand to metal donation. It is, indeed, characterized by a charge density depletion (red isodensity) at the $CN^-$ site whereas a charge accumulation (blue isodensity surface) is present at the metal fragment. It is worth noting that this charge accumulation has a toroidal shape, exhibiting a two-lobed isodensity surface with a depletion region along $z$. The charge depletion at the $CN^-$ site brings to mind the shape of the $\sigma$-symmetry HOMO[1] of the free $CN^-$ fragment whereas the charge rearrangement at the metal site appears related in shape to the unoccupied spherical $s$ orbital of $M^+$, slightly distorted due to the hybridization with the filled d-shell. We mention that the $\Delta\rho'_1$ contribution bears, at least from the topological point of view, a striking similarity to a $\sigma$ orbital contribution to the bond in AuCN and referred by Zaleski et al.[40] as the "doughnut hybrid".

The presence of the s-d hybridization, just mentioned, is evident if we look at the separated NOCV densities $\{|\Phi_{-1}|^2,\ |\Phi_{+1}|^2\}$, also reported in the Figures. We recall that a NOCV-pair density $\Delta\rho'_k$ ($\Delta\rho'_k = v_k(|\Phi_{+k}|^2 - |\Phi_{-k}|^2)$) in the NOCV theory can be interpreted as arising by a charge transfer from the $\Phi_{-k}$ spin-orbital to the $\Phi_{+k}$ spin-orbital (actually, here, $\Phi_{\pm k}$ are four-component spinors, see the section on Methodology). The corresponding eigenvalue $v_k$ is the actual amount of electron charge transferred. Thus, it is clear that the charge accumulation of toroidal shape observed at the coinage metal site is entirely due to $|\Phi_{+1}|^2$, which is exclusively localized at the metal site, whereas $|\Phi_{-1}|^2$ (related to the electron density depletion) is more delocalized with contributions both from $CN^-$ and from the metal itself. Thus, the picture that emerges is clear, the charge accumulation observed at the metal site unmistakably arises both from a charge transfer from $CN^-$ and also as a flux of charge entirely localized within the metal (polarization), which comes from the filled $d$ metal orbitals that lie along the internuclear axis. This pattern of charge rearrangement is exactly

[1]Even though in the relativistic framework orbitals have been substituted with spinors, we retain the familiar acronym HOMO

what one would expect from the s-d hybridization mechanism. In fact we can consider it a sort of fingerprint of the $s-d$ hybridization in coinage metals (we will return on this point in the next section). We just note for now that the qualitative pattern is the same for all coinage metals.[38] However, one may expect some quantitative differences between different metals as suggested by the respective NOCV eigenvalue $v_1$ (see Table1).

The second NOCVs-pair density ($\Delta\rho'_2$), is more difficult to correlate with the classical donation and back-donation constituents of the DCD model. It accumulates electron density between the metal and the carbon atom of $CN^-$. It bears witness to the effect of antisymmetrization, in the sense that this pair contribution involve only a slight charge reorganization which seems roughly to balance the $\Delta\rho^{anti}$ term. We mention that Frenking et al. suggested, in the case of coinage metal carbonyl complexes ($MCO^+$), that this component may be also related with an unconventional (not considered in the DCD model) $\sigma$-backdonation.[32]

The last two contributions $\Delta\rho'_3$ and $\Delta\rho'_4$ have to be clearly attributed to a small back-donation from the metal to the ligand. They are characterized by a small electron density depletion at the metal site and a significant charge accumulation at the carbon site. Superimposed to this back-donation is a significant polarization of $CN^-$ (charge flux from N to C) induced by the positive charge on the metal. Some differences between complexes can be highlighted. In the case of AgCN, the electron density depletion observed at the metal is actually very small, whereas it is more pronounced in CuCN, with $\Delta\rho'_3$ and $\Delta\rho'_4$ exactly overlapped. In the case of AuCN, the depletion observed at the metal is even greater and $\Delta\rho'_3$ and $\Delta\rho'_4$ are not superimposable, with $\Delta\rho'_3$ presenting a more significant depletion at the metal site than $\Delta\rho'_4$.

All the previous considerations can be revisited at a quantitative level with help of the CD functions (see Figure4). We recall here that at a given point along a chosen axis (here, the molecular axis), $z$, a positive value of the CD function indicates a corresponding flow of electrons from the right to the left; in our case from the $CN^-$ towards the metal M. Conversely, a negative value of the CD function corresponds to a transfer in the opposite

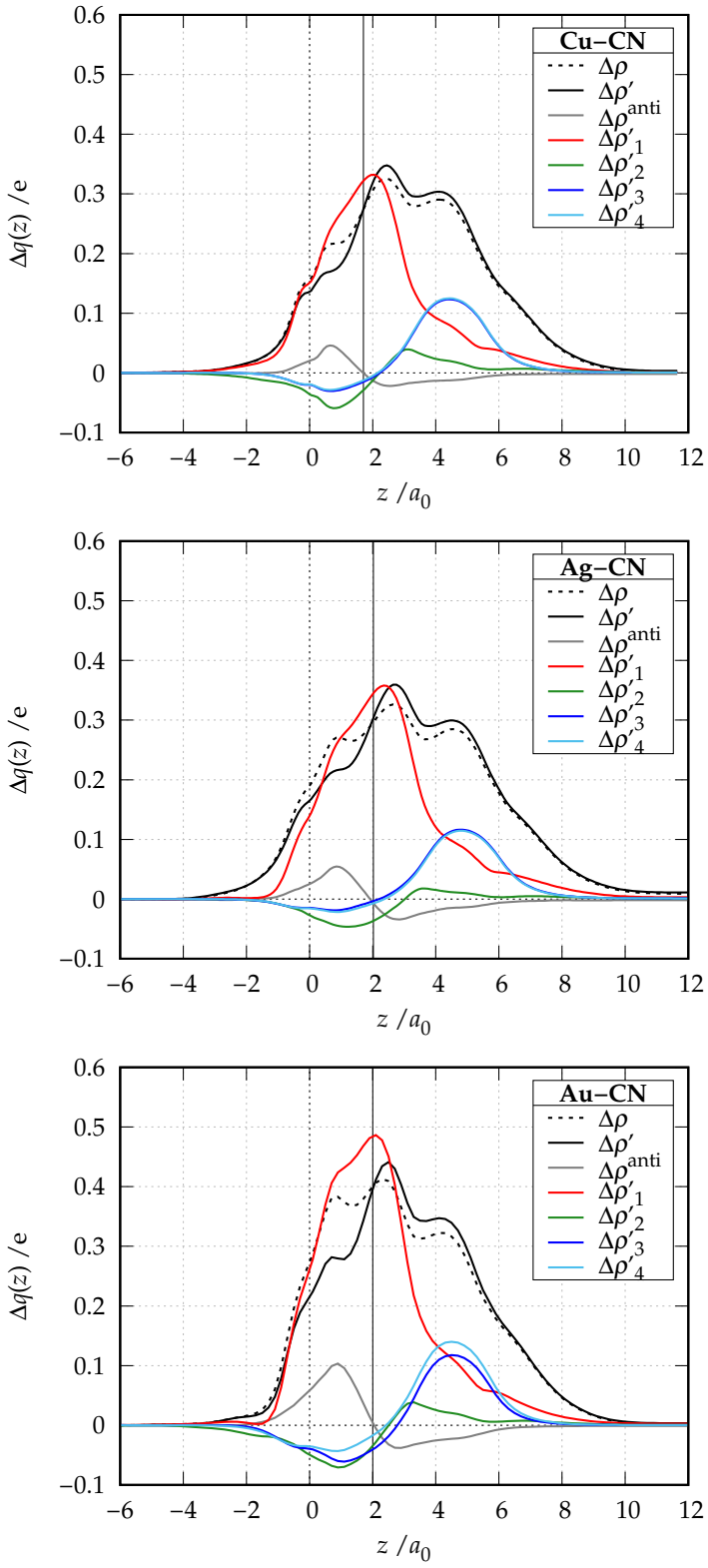


Figure 4: Charge-displacement curves for the MCN complexes, M=Cu, Ag, Au. The vertical line marks the boundary between the $M^+$ and the $CN^-$ fragment (see text for details). Distances are reported in bohr ($a_0$).

direction, that is from the metal $M^+$ to $CN^-$. A reasonable measure of the charge transfer (CT) between the $CN^-$ and $M^+$ fragment is easily obtained by fixing a plausible boundary to separate the fragments within the complex. Our standard choice is the $z$-point where equal-valued isodensity surfaces of the isolated fragments become tangent.[20,29,46] The vertical black line in the Figures marks this "isodensity boundary".

The CD functions associated with the overall electron density rearrangement (labeled as $\Delta\rho'$ and $\Delta\rho$, continuous and dashed black lines, respectively) show a positive value in the whole molecular region, indicating a net flow of electrons from $CN^-$ towards the metal. The CD function for $\Delta\rho$ is everywhere higher than the corresponding antisymmetrized one ($\Delta\rho'$) on the left of the boundary, and lower on the right. Thus, the function for $\Delta\rho'$ features a greater slope at the isodensity boundary, indicating a larger accumulation (smaller depletion) of charge density in the bonding region than $\Delta\rho$. Despite of these differences, the net CT one extracts from these two curves is essentially the same (to within 0.01 e) because they cross each other very close to the isodensity boundary (see also Table 1). The net CT increases significantly going down the periodic table (i.e. 0.27 e, 0.30 e and 0.40 e in CuCN, AgCN and AuCN, respectively), with the gold cation that presents the strongest net withdrawing ability among coinage metals.

The CD functions associated with the NOCV components, $\Delta\rho'_k$ (colored lines), are also shown for all systems in Figure 4. The CD function for $\Delta\rho'_1$, shown as a red line, is positive in the whole molecular region, and reaches its maximum roughly at the boundary. This gives us a detailed picture of the metal←ligand donation. The charge flow from $CN^-$ to $M^+$ amounts of 0.322, 0.345 and 0.484 e for CuCN, AgCN and AuCN, respectively ($CT_1$), as reported in Table1. The green CD curve of $\Delta\rho'_2$ accounts for charge density accumulation in the bonding region, because of its positive slope, while a maximum and minimum appear nearby the position of $M^+$ and C respectively, elsewhere the curve is almost flat. As mentioned above, this CD does not exhibit an evident counterpart in the DCD bonding model: the curve describes an electron density accumulation in the M-CN bonding region with a small

CT between the fragments (the curve crosses the zero axis in a region between the fragments, close to the isodensity boundary). Therefore, the CT values are small for all systems ($CT_2$ ranges from -0.029 e of CuCN to 0.036 e of AgCN). Note also that the CD roughly mirrors the $\Delta\rho^{anti}$ curve, also reported in the figure.

The last two CD functions associated to $\Delta\rho'_3$ and $\Delta\rho'_4$ are negative at the $M^+$ site and clearly quantify the metal→ligand back-donation. On the $CN^-$ fragment the CD curves have a bell shape, describing a large polarization of the cyanide group (displacement of electrons from nitrogen towards carbon) due to the presence of the positively charged metal cation. Despite of this charge flux is in the opposite direction to the back-donation, the CD curves remain negative at the isodensity boundary. The CTs for these components are similar (-0.015 and -0.013 $e$) in the case of CuCN, almost negligible (-0.003, -0.007 e) for AgCN and significantly larger (0.041 and 0.017 e) for AuCN. The removal of degeneracy in the two back-donation components in the case of gold is clearly due to the spin-orbit coupling effect, which locally breaks the degeneracy of the $5d$ Au atomic orbitals ($5d_{j=3/2}$ and $5d_{j=5/2}$ spinors, which differ both in energy and spatial distribution[47]) and, quite surprisingly, extends its effect to the Au-C bond region and even to the CN site.[48] We mention that the remaining NOCV components are of negligible interest, because of their associated CD curves are non-zero only within the fragments (for example the CD curves for $\Delta\rho'_5$ and $\Delta\rho'_6$ in the case of AuCN are reported in Figure S1 of the SI). Summarizing, our NOCV/CD analysis shows that the gold has both the largest donation and, although small in absolute value (due to the negative charge on $CN^-$ that does not make it a good electron acceptor ligand), the largest back-donation amongst the noble metals. This finding supports the picture that gold tends, more than the other coinage metals, to form multiple bonds.

Before concluding this section, it is interesting to investigate the effect of relativity on the bonding components in the AuCN complex. We performed the NOCV/CD analysis increasing, in the relativistic hamiltonian, the speed of light by one order of magnitude (c = 10×137.036 a.u.) to simulate the non-relativistic limit. The results clearly show that

the DCD components of the coordination bond in AuCN are substantially altered when relativistic effects are switched off. In particular, the ligand-to-metal donation decreases by more than a third (passing from 0.48 to 0.31 e) and the overall back-donation is smaller (0.02 e) and split into two equal contributions, because in the absence of spin-orbit coupling $\Delta\rho'_3$ and $\Delta\rho'_4$ are essentially identical. Thus, a "non-relativistic gold" would give gold-carbon bonds of comparable character to those of silver and copper. It is interesting also to note that, in contrast with what we have just seen for the metal-carbon bond components, the polarization of the C-N bond is only marginally affected by relativity.

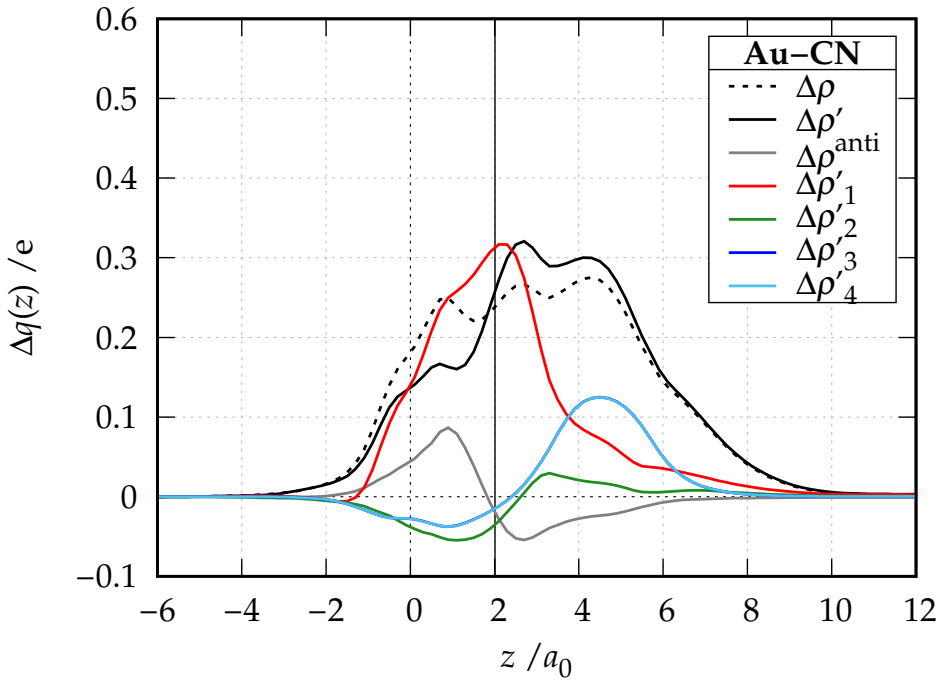


Figure 5: Charge-displacement curves for the AuCN complex, increasing speed of light $c$ by a factor of ten and approaching the non-relativistic limit. The vertical line marks the boundary between the $Au^+$ and the $CN^-$ fragment (see text for details). Distances are reported in bohr ($a_0$).

One may expect that the relativistic effects have a significant impact on the electron density rearrangement within the metal fragment and in particular on the component, $\Delta\rho'_1$. This is because, as mentioned above, the behavior of this component in the Au region is strictly related to the s-d hybridization mechanism, which is indeed expected to be significantly

reduced if relativistic effects are neglected. Relativistic effects favor s-d mixing, leading to a stabilization/contraction of the 6s shell, and a destabilization/expansion of the 5d shell. The fact that the relativity is important for s-d hybridization is suggested by the value of $v_1$, which is significantly reduced on passing from the full relativistic regime (0.965) to the non-relativistic limit (0.608 e). This reduction is larger than what we may expect on the basis of the sole decrease of the donation component. In the next section we shall give a more quantitative measure of the electronic flux involved in the s-d hybridization mechanism, with the increase of relativistic effects going down the coinage metal series.

## Mechanism of s-d hybridization in CuCN, AgCN and AuCN

While the concept of $sp^n$ hybridization of main-group atoms and their correlation with molecular structures is well-known and is a standard part of chemistry textbooks, the s-d hybridization occurring in transition metals compounds is much less familiar,[49] even if has been outlined since the middle of the last century.[50,51] The s-d hybridization is often advocated to explain peculiar structural properties of gold-containing molecules or clusters. The mixing of 5d and 6s orbitals has been proposed as a chief cause for the higher tendency of gold(I) to form linear complexes compared to copper(I) or silver(I). As mentioned in the introduction, this mechanism, moving charge from the internuclear axis to the spherical empty s orbital, is expected to have a significant impact on the metal-ligand distance. Since the $5d_{z^2}$ and 6s orbitals are closer in energy in gold than in copper or silver because of relativity, the s-d mechanism is thought to be more important for gold than for other coinage metals. However, despite its potential importance in determining and rationalizing structures, a quantitative assessment of the degree of hybridization (how many electrons are expected to be involved) is very scarce even in simple systems. A notable exception is the pioneering work of Fan et al.,[43] which indeed inspired the present contribution.

The following questions arise: i) Is it possible to give a quantitative measure of the s-d hybridization for the M-CN systems? ii) Does s-d hybridization occur in the case of the

lighter coinage metals, i.e. copper, silver or is it peculiar of gold? iii) How is s-d hybridization quantitatively reflected in observable properties of the coordination bond? Concerning the first point, the NOCV analysis, presented above, suggests a very simple and straightforward method for assessing the degree of s-d hybridization in noble-metal cyanides. In particular, the electron density depletion in the inner part of the metal, which has the shape of an atomic $n\mathrm{d}_{z^2}$ orbital (see the $|\Phi_{-1}(x,y,z')|^2$ 3D plot contribution to $\Delta\rho_1$ in Figures 1, 2 and 3), and the concurrent electron density accumulation (of toroidal shape) taking place exclusively at the metal ($|\Phi_{+1}(x,y,z')|^2$) can be regarded as the fingerprint of the s-d hybridization mechanism. Thus, a natural choice to quantify these effects is to analyze separately these NOCV pairs by means of the charge displacement function. In particular, NOCV pairs scaled for their eigenvalues (i. e. $v_1|\Phi_{+1}(x,y,z')|^2$ and $-v_1|\Phi_{-1}(x,y,z')|^2$) are analized. By definition, these functions add up to the charge displacement function associated with $\Delta\rho_1$. The results are reported, for all systems, together with the related 3D isodensity plots in Figure 6. The CD curves, from their zero value, are monotonically increasing for $v_1|\Phi_{+1}(x,y,z')|^2$ and decreasing for $-v_1|\Phi_{-1}(x,y,z')|^2$ up to their asymptotic values ($+v_1$ and $-v_1$, respectively). As already mentioned above, the $|\Phi_{-1}|^2$ NOCV consists of two distinct portions: one is a decrease of electron density (recalling the $d_{z^2}$ shaped lobe) entirely located on metal fragment along the internuclear axis, whereas the other, located on the cyanide moiety resembles the $\sigma$-HOMO orbital of $CN^-$. The isodensity boundary is precisely located in between. Thus, considering the red curve, we see that the boundary, is located in a nearly flat region of the curve, confirming that these two portions can be unambiguously separated. The value that the CD function associated with $|\Phi_{-1}|^2$ assumes at this boundary point measures the amount of electronic charge which is transferred from the $d_{z^2}$ shaped portion of $\Phi_{-1}$ to $\Phi_{+1}$. The latter is entirely located on the metal center (this is confirmed by the fact that the $\Delta q$ value at the boundary for $\Phi_{+1}$ has already reached its asymptotic value of $v_1$).

The picture that emerges is clear: the accumulation at the gold site (almost 0.95 electrons, this value is very close to the numerical value of $v_1$) is due not only to a large charge transfer

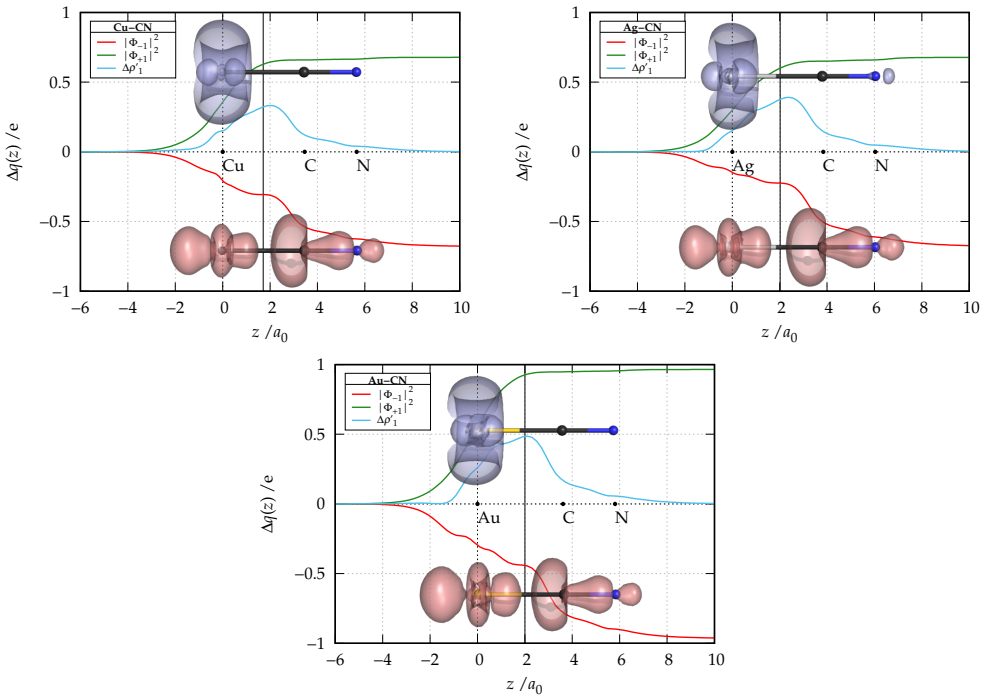


Figure 6: Charge-displacement curves for the MCN complexes, M=Cu, Ag, Au. The curves labeled as $|\Phi_{-1}|^2$ and $|\Phi_{+1}|^2$ are scaled for the respective NOCV aigenvalue ($v_1$). The dots on the axis mark the z coordinate of the atoms, with the M atom being at the origin of the axis. The vertical line marks the boundary between the $M^+$ and the $CN^-$ fragment (see text for details). The parent NOCV-pairs densities $|\Phi_{-1}|^2$ and $|\Phi_{+1}|^2$ are also reported by means of isodensity surfaces ($\pm$ 0.005). Red surfaces identify charge depletion areas, blue surfaces identify charge accumulation areas.

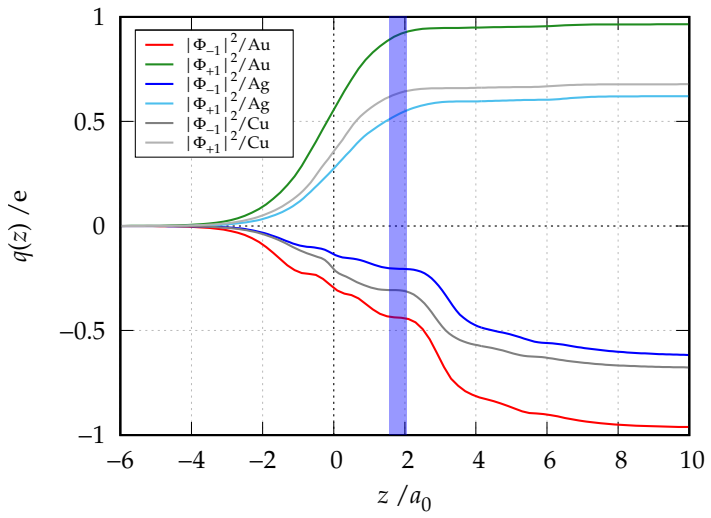


Figure 7: Comparison of charge-displacement curves of parent NOCV-pairs densities $|\Phi_{-1}|^2$ and $|\Phi_{+1}|^2$ for the MCN complexes, M=Cu, Ag, Au. The narrow vertical band shows include the position of the isodensity boundary for all systems.

from $CN^-$ (0.48 e) but also to the s-d hybridization (0.45 electrons which upon the bond formation are transferred from the $(n-1)d$ to the $ns$ orbitals).

Turning now to the question of the presence and relative importance of s-d hybridization for the three coinage metals, we show in Figure 7 the CD curves corresponding to the NOCV pair $\{|\Phi_{-1}|^2, |\Phi_{+1}|^2\}$ for each M-CN (M=Au,Ag,Cu), in a single graph for easier comparison. As expected, gold features the largest degree of hybridization among coinage metals, yet our analysis shows unequivocally that, although to a smaller extent, s-d hybridization mechanism occurs also in the other metals. Quantitatively, the values extracted from the CD functions are 0.33 and 0.20 electrons for copper and silver, respectively. Thus, the amount of $d$ electrons transferred is greater in case of Cu than Ag. Noteworthy, the trend is consistent with the energetics of (n-1)$d^{10}$-(n-1)$d^9$n$s^1$ electronic transition for the coinage metal cations (i.e. it has the largest value for silver (4.86 eV) , and the smallest for gold (1.86 eV), with copper (2.72 eV) in between).[52]

Now, we would like to briefly address the interesting point of how s-d hybridization tangibly affects bond formation. A simple effect that one might expect is on the bond

distances. Since $nd_{z^2}$ electrons move out of the molecular axis and density depletion occurs, in an almost symmetric fashion towards and away of the approaching $CN^-$, one may expect that the repulsive barrier also weakens symmetrically, which would result in a tendency to have shorter bond distances and to form linear structures.[39,53] This is indeed the case of gold(I) that has, among the coinage metals, the largest ability to form linear complexes, with significant consequences on its catalytic activity. We could also simply rephrase this by saying that the effective shape of the coinage metal is flattened by the action of s-d hybridization. We explore this here by comparing the relevant features of the electronic density at the metal site in AuCN with those of the isolated cation $Au^+$. The corresponding results for CuCN and AgCN are reported in the SI.

In Fig. 8 we compare the electron density profile of AuCN (solid line) along the $z$ axis with that of the spherical isolated $Au^+$ cation, placed at the same position it assumes in the molecule. For AuCN, the flattening of Au emerges clearly: the density profile of the AuCN molecule is indeed systematically lower than that of the isolated spherical cation $Au^+$. Surprisingly, this means that for an approaching ligand in trans position to CN, the gold atom appears even smaller than the bare cation, $Au^+$. Intuitively, this situation favors a closer approach of ligand in trans. In order to be more quantitative, we introduce the $\Delta z$ parameter,[54] as a measure of the reduced size of the metal. The $\Delta z$ is defined as the distance between two equal-valued density profile points (one for $Au^+$ and the other for AuCN). If as reference density value we consider that which obtained at the ionic radius of $Au^+$, we find that this value in AuCN is obtained at a significantly shorter distance $\Delta z = 0.21$ bohr (0.11 Å). This effect follows the trend of s-d hybridization and it is found to be reduced in the other coinage metals ($\Delta z = 0.08$ bohr and 0.04 bohr for CuCN and AgCN, respectively), see Figures S2 in SI.

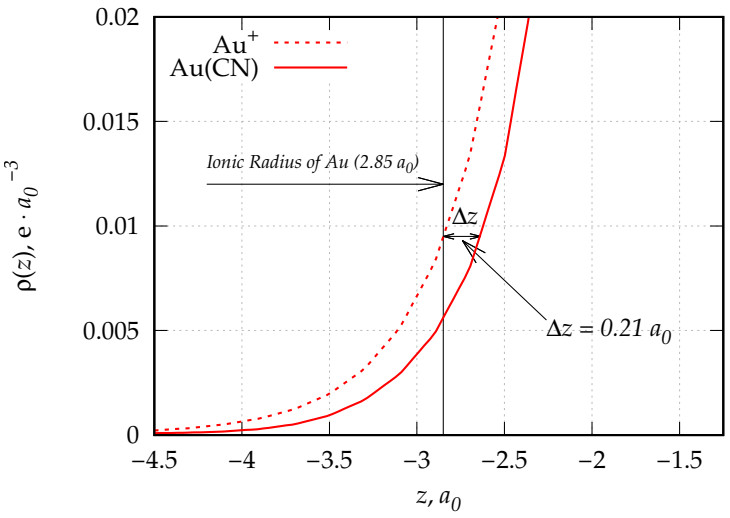


Figure 8: The electron density profile, $\rho$ ($e$ bohr$^{-3}$) along the $z$ axis of AuCN (solid line) and of the spherical $Au^+$ atom (dotted line), placed a the the same position which assumed in the molecule. $\Delta z(a_0)$ is defined as the distance between two points of density profiles taking the same density value. The isodensity value has been chosen as that corresponding the ionic radius of $Au^+$ and thus representing a suitable cation surface. The reference atomic radius has been obtained from Ref.[55] (see also http://abulafia.mt.ic.ac.uk/shannon/).

## Ligand effect: s-d hybridization vs size effect.

In the above section we showed that s-d hybridization, promoted by an approaching ligand ($CN^-$), has a significant effect on the effective size of the metal in trans position. This poses the issue if and how this mechanism is affected by the nature of the promoting ligand (e.g. electron donating ability, charge or the nature of the atom directly bound to gold). This is clearly of relevance for understanding the basic mechanism of the hybridization process and also in the field of gold catalysis where typical gold(I) catalysts have a basic formula, $[Au(I)\text{-}L]^{+/0}$. Thus, in this section we report a comparative analysis of the s-d hybridization that occurs at $Au^+$ in different Au(I) metal fragments of general formula $[AuL]^{+/0}$, where L is chosen from some ligands frequently used both in coordination and in organometallic chemistry (L=$F^-$, NHC, CO, $PH_3$ and Ne, where NHC is imidazol-2-ylidene). The noble gas Neon has been added as a limit case of weak perturber of the bare gold cation $Au^+$.

As above, we evaluate the charge displacement function associated with $|\Phi_{-1}|^2$ (see Figure

9) for all systems. The amount of electronic charge which is transferred ($\Delta_{hyb}$) from the $5d_{z^2}$ shaped portion of $\Phi_{-1}$ to $\Phi_{+1}$ is given in Table 2. In the same table we also report the total CT and the donation component ($CT_{don}$) between ligand and $Au^+$ and related to $\Delta\rho_1$. As expected, in the $[Au(Ne)]^+$ model case, the amount of s-d hybridization is very small (0.07 e), however it has to be noted that this value is even larger than the net Ne$\rightarrow$ $Au^+$ CT (0.03 e). The variability of $\Delta_{hyb}$ for the others ligands is significant: it ranges from 0.295 e to 0.574 e for $PH_3$ and $F^-$, respectively. Our results show that there is no clear correlation between the donor ability of the ligand (both net CT and $CT_{don}$) and $\Delta_{hyb}$ (amount of s-d hybridization). For example, $PH_3$, which has the greatest donation capability ($CT_{don} = 0.54$ e), presents the least ability to induce s-d hybridization (with the exception of Ne, it has the lowest $\Delta_{hyb}$ value). The s-d hybridization in gold thus appears mainly sensitive to the nature of the atom directly bound to the metal more than others factors such as the net charge of the ligand or its donor ability. For instance, the group of three carbon-containing ligands, namely CO, NHC, $CN^-$, all have very similar values of $\Delta_{hyb}$ despite of the fact they have a different charge, electron donor ability (CO has a modest ability in donating electron charge to the metal compared to NHC or $CN^-$, see the $CT_{don}$ and $CT_{net}$ values in Table2) or carbon hybridization (carbon is hybridized *sp* in CO and $CN^-$ and $sp^2$ in NHC).

As we already noted above, since s-d hybridization moves *d*-electrons out of the molecular axis in a symmetric fashion (both in the direction of the ligand and in trans position) and density depletion occurs at the metal, a substrate approaching from the left is expected to get closer to gold, since the repulsive barrier weakens. The distance of approach is expected to be shorter in proportion to the degree of hybridization. This should translate into some relation between the flattening of the gold atom in trans position (as measured by the $\Delta z$ parameter) and the degree of hybridization (evaluated as $\Delta_{hyb}$). Figure 10 shows that such a trend indeed exists.

Table 2: The total CT, the donation component ($CT_{don}$) between ligand and $Au^+$ and electronic charge associated with s-d hybridization ($\Delta_{hyb}$) (values are reported in electrons, e). $\Delta z$ parameter (see text) is reported in bohr ($a_0$).

| | $CT_{don}$/e | $CT'_{net}$/e | $\Delta_{hyb}$/e | $\Delta z/a_0$ |
|---|---|---|---|---|
| $[Au(Ne)]^+$ | 0.031 | 0.032 | 0.071 | 0.008 |
| $[Au(PH_3)[^+$ | 0.574 | 0.425 | 0.295 | 0.165 |
| $[Au(CO)]^+$ | 0.348 | 0.149 | 0.383 | 0.210 |
| AuCN | 0.484 | 0.395 | 0.442 | 0.207 |
| $[Au(NHC)]^+$ | 0.489 | 0.398 | 0.422 | 0.219 |
| AuF | 0.381 | 0.409 | 0.574 | 0.229 |

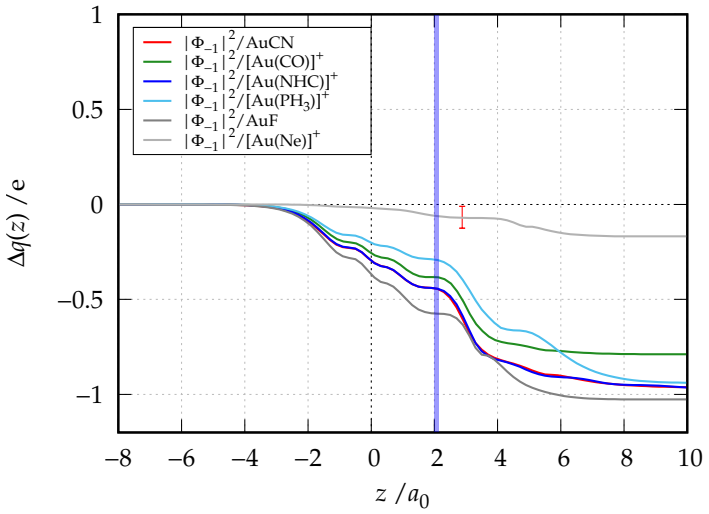


Figure 9: Comparison of charge-displacement curves of NOCV density $|\Phi_{-1}|^2$ for $[AuL]^{+/0}$, where L=$F^-$, NHC, CO, $PH_3$ and Ne. The narrow vertical band shows include the position of the isodensity boundary for all systems ( except for $[Au(Ne)]^+$, whose isoboundary is highlighted by red vertical bar).

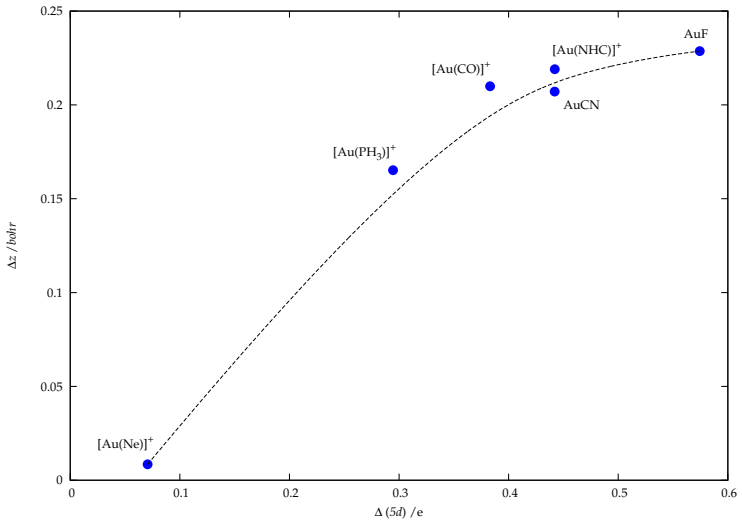


Figure 10: $\Delta z$ reported with respect the amount of $\Delta_{hyb}$, electrons transferred from $d_{z^2}$ orbital. $\Delta z$ has been evaluated keeping the density $\rho$ fixed at 0.01 a.u. Distances are bohr ($a_0$).

# Conclusion

We have carried out in this work an original and insightful theoretical analysis of the coordination bond between coinage metal cations ($Cu^+$, $Ag^+$ and $Au^+$) and the cyanide ion ($CN^-$).

The analysis was carried out using four-component relativistic density functional theory and based on the charge-displacement/natural orbitals for chemical valence (CD-NOCV) scheme. The analysis permits a rigorous definition and assessment of the bonding components at the heart of the popular Dewar-Chatt-Duncanson model: substrate-to-metal donation and metal-to-substrate back-donation. We conclusively show that M-CN bond is characterized by a large donation from the cyanide ion to the metal cation and two small back-donation components from the metal towards the cyanide anion. In comparison with the other coinage metals, gold has both the largest donation (30%-40% better acceptor than Cu and Ag, respectively) and the largest back-donation. Furthermore, the CD/NOCV scheme used in combination with full relativistic four-component approach, clarifies that relativity plays a crucial role for the Au–CN bond: it enhances the multiple bond character in

gold and the spin-orbit coupling, removing the degeneracy of the 5d atomic orbitals, induces a substantial split in the back-donation components, which propagate, to some extent, to the charge rearrangement at the cyanide site.

Finally, we conclusively answer some long-standing questions concerning s-d hybridization in coinage metals. A simple spatial analysis of the NOCV pair densities related to the ligand to metal donation allowed us to assess with an unprecedented accuracy the charge rearrangement involved with the s-d hybridization occurring at the metal upon its interaction with the cyanide anion. Contrary to a widely held view, s-d hybridization is present in all noble metal complexes, and it is significantly enhanced in gold because of relativity. We found that s-d hybridization plays a key role in determining the shape and size of the metal: it removes electron density from the bond axis and induces a significant flattening at the metal site in trans position to the ligand. This influences the bond distances in all coinage metal complexes, however its effect is found to be larger for Au, which is consistent with the preference of gold to form linear complexes. A comparative investigation on simple complexes $[AuL]^{+/0}$ of $Au^+$ bearing different ligands (L=$F^-$, N-Heterocyclic Carbene, CO, PH3 ) shows that the s-d hybridization mechanism is influenced by the nature of the ligand. In particular we ascertained that the major influence is exerted by the nature of the atom directly bound to the metal, and only to a marginal extent by other features, such as the net charge of the ligand or its donor ability. Thus, for example, the three carbon-containing ligands, namely CO, NHC, $CN^-$ induce all very similar s-d hybridization of $Au^+$ despite the fact that they have different charges, electron donor ability or carbon hybridization.

The tools presented in this work appear to be particularly powerful for understanding the electronic structure of molecular systems containing heavy elements. Clearly, this methodology can of course be applied to more complex systems, such as organometallic complexes, to guide the tuning of the metal-substrate bond properties through a suitable combination of donor/acceptor properties of the ligands or to super-heavy-metal compounds[56,57] where relativistic effects, including spin-orbit coupling, are expected to be even more important.

# Methods and Computational Details

## Charge-displacement analysis via natural orbitals for chemical valence (CD-NOCV) in the four-component relativistic framework

The Charge-Displacement (CD) analysis,[29] is a powerful tool that allows to measure the exact amount of electron density that, upon formation of a bond between two fragments, is transferred from a fragment to another. The method has extensively been employed to analyze the nature of intermolecular interactions with particular focus on the charge-transfer component.[46] The CD function is defined as a partial progressive integration along a suitable $z$ axis of the difference $\Delta\rho(x, y, z')$ between the electron density of the adduct and that of its non-interacting fragments placed at the same position they occupy in the adduct:

$$\Delta q(z) = \int_{-\infty}^{z} dz' \int_{-\infty}^{\infty}\int_{-\infty}^{\infty} \Delta\rho(x, y, z')dxdy. \quad (1)$$

In the previous equation the integration axis is conveniently chosen as the bond axis between two fragments constituting the adduct. In this work the fragments are the coinage metals cations ($Cu^+$, $Ag^+$, $Au^+$) and cyanide anion ($CN^-$). The CD function quantifies at each point of the bond axis the exact amount of electron charge that, upon formation of the bond, is transferred from right to left across a plane perpendicular to the bond axis through $z$. Negative values of the CD function identify charge flow in the opposite direction. To be able to define CT in this context, we need to take the CD value at some specific point between the fragments (i.e, at an arbitrary defined plane separating them). The usual choice, which is at the so-called "isodensity boundary", is the $z$ point where equal-valued isodensity surfaces of the isolated fragments become tangent.

A particularly useful feature of the CD function is its partitioning. If the complex and its constituting fragments belong to the same symmetry group, the electron density difference can be decomposed into additive symmetry components according to the different

irreducible representations of their symmetry point group.[58] The symmetry decomposition of the electron density difference induces similarly a decomposition of the CD function which, for suitable cases when the symmetry components identify the Dewar-Chatt-Duncanson components, gives a precise picture of donation and back-donation charges.[19,31,48,58,59]

In more general cases, particularly when the complex and its constituting fragments have no symmetry (or as in the present case the symmetry is reduced due to inclusion of spin-orbit coupling), the CD function can be also decomposed by introducing the Natural Orbitals for Chemical Valence (NOCV) scheme. Natural orbitals for chemical valence (NOCV) were introduced by Mitoraj and Michalak[60,61] as descriptors of chemical bond. The NOCV formalism allows a very compact description of the bonding phenomenon because the electron density difference can be brought into diagonal contributions in terms of NOCVs. The analysis approach they provide was shown to be particularly valuable for transition metal complexes: in this case the NOCV provide quantitative characterization of $\sigma$-donation and $\pi$-back-donation effects contributing to metal-substrate bond. In the CD-NOCV framework,[62] the charge rearrangement taking place upon bond formation is obtained from the occupied orbitals of the two fragments suitably orthogonalized to each other and renormalized (promolecule).

The resulting electron charge density rearrangement $\Delta\rho^{'}$ can be written in terms of NOCV pairs orbitals $\{\phi_k,\ \phi_{-k}\}$, that are the eigenfunctions of the so-called "valence operator" of Nalewajski and Mrozek valence theory[63,64] as follows

$$\Delta\rho' = \sum_k v_k(|\phi_k|^2 - |\phi_{-k}|^2) = \sum_k \Delta\rho'_k \tag{2}$$

This above relation guides us in the interpretation of the NOCVs ($\phi_{\pm k}$) and their associated eigenvalues ($v_{\pm k}$): upon formation of the adduct from the promolecule, a fraction $v_k$ of electrons is transferred from $\phi_{-k}$ to the orbital $\phi_k$. It can be shown from the definition of the operator $\hat{V}$ that $k$ ranges from 1 to number of occupied spinors. Moreover it is

important to notice that only a small subset of these NOCV pairs actually contributes to the overall rearrangement $\Delta\rho'$ because a large part of them presents values of $v_k$ close to zero. The CD-NOCV approach has been successfully applied for the characterization of transition metal compounds and for disentangling donation and back-donation in the CD function of nonsymmetric systems containing NHC-Au(I) bond[65] or Au(III)-CO bond with different ancillary ligands.[66]

CD-NOCV analysis turns out to be formulated in a very general fashion regardless the specific theoretical method of how the electron density is calculated, thus its relativistic four-component generalization was simple. In this work, we use its implementation recently carried out[67] in the Dirac-Kohn-Sham module of the code BERTHA.[68–70]

We only mention that the electron density we use corresponds to the total electron charge-density of a single determinant:

$$\rho(\boldsymbol{r}) = \sum_i \boldsymbol{\Psi}_i^\dagger(\boldsymbol{r}) \cdot \boldsymbol{\Psi}_i(\boldsymbol{r}) = \sum_i \rho_i(\boldsymbol{r}) \tag{3}$$

where $\Psi_i$ is the four-component spinor solution of the DKS equation. The resulting density rearrangement that we shall identify with $\Delta\rho'$, being the reference antisymmetrized now reads in terms of spinors

$$\Delta\rho' = \sum_i^N |\boldsymbol{\Psi}_i^{(AB)}|^2 - \sum_i^N |\boldsymbol{\Psi}_i^0|^2 \tag{4}$$

where $\boldsymbol{\Psi}_i^{(AB)}$ are the occupied molecular spinors of the adduct and $\boldsymbol{\Psi}_i^0$ are obtained from the occupied spinors of A and B properly orthogonalized to each other and renormalized.

In analogy with Eq.2, $\Delta\rho'$ can be decomposed exactly in NOCV-pairs density ($\Delta\rho' = \sum_k v_k(|\boldsymbol{\Phi}_k|^2 - |\boldsymbol{\Phi}_{-k}|^2) = \sum_k \Delta\rho'_k$), where $\boldsymbol{\Phi}_k$ and $v_k$ are the spinor eigenfunctions and eigenvalues of the generalized chemical valence operator

$$\hat{V} = \sum_{i=1}^N (|\boldsymbol{\Psi}_i^{(AB)}\rangle\langle\boldsymbol{\Psi}^{(AB)}| - |\boldsymbol{\Psi}_i^0\rangle\langle\boldsymbol{\Psi}_i^0|). \tag{5}$$

We mention that, because the molecular systems we considered here are all closed-shell, as are the respective fragments, the NOCV spinors arise naturally as Kramers pairs with degenerate eigenvalues which, for clarity of presentation, have been summed. All details of the implementation can be found in Ref.[67]

## Computational details

Calculations were carried out with a recently implemented full-parallel version of the program BERTHA.[71,72] The program BERTHA and its main relevant features have been described in the previous section and references therein. The large component of the basis set for Au and Ag was generated by uncontracting triple-$\zeta$ quality Dyall's basis sets[73–76] augmented with the related polarization and correlating functions. Final basis set schemes are as follows: Au $(30s24p15d11f5g1h)$, Ag $(28s20p13d7f3g)$. Large component basis functions for Cu, P, N, C and H were derived by decontracting the related aug-cc-pVTZ-DK[77–79] basis sets available at the "Basis Set Exchange" site.[80] The corresponding small component basis was generated using the restricted kinetic balance relation.[81] For gold, a previously optimized auxiliary basis set for density fitting denoted as B20[82] was used. For all other elements namely Cu, Ag, P, N, C and H, accurate auxiliary basis set were generated using a simple procedure starting from available DeMon Coulomb fitting basis set. It is worth recalling that the Hermite Gaussian Type Functions (HGTFs) used as fitting functions, are grouped together in sets sharing the same exponents (an analogous scheme is adopted in the non-relativistic DFT code DeMon[83]). The sets are formed so that to an auxiliary function of a given angular momentum all the functions of smaller angular momentum are associated. Consequently, due to the variational nature of the density fitting procedure implemented, a fitting basis set of increased accuracy can be generated by simply up-shifting the angular momentum in the basis set definition.[84] For Cu and Ag we achieved a fitting basis set of higher accuracy (referred to as A2) simply by up-shifting of two units the angular momentum of all the DeMon Coulomb Fitting definitions. For the sake of clarity we give the dimension

of the C-atom (or equivalently N-atom) auxiliary basis sets, which is (7s,7p,7d,3f,3g). This assures an accuracy on the Coulomb energy of 0.03 mHartree. The BLYP functional made of the Becke 1988 (B88) exchange[85] plus the Lee-Yang-Parr (LYP) correlation[86] was used. An energy convergence criterion of $10^{-7}$ Hartree on the total energy was adopted. For the metal cyanides (MCN, with M=Cu, Ag, Au), data were obtained using the gas-phase experimental equilibrium geometry.[40] In the case of AuF and $AuNe^{+}$ we used the geometry optimized at Coupled Cluster level and obtained from Ref.[29] and Ref.,[87] respectively. The geometry of the systems $[AuL]^{+}$, with L=PH3, NHC have been obtained by means of full geometry optimizations at BLYP/TZ2P level using ADF code with the ZORA hamiltonian.[88]

## Acknowledgement

The Ministero Istruzione dell'Università e della Ricerca (MIUR) and the University of Perugia are acknowledged for the financial support through the program "Dipartimenti di Eccellenza 2018-2022" (grant AMIS). LS thanks University of Chieti-Pescara for financial support.

## Supporting Information Available

Geometries of the studied complexes are reported in XYZ format. This material is available free of charge via the Internet at `http://pubs.acs.org/`.

## References

(1) Patterson, H. H.; Kanan, S. M.; Omary, M. A. Luminescent homoatomic exciplexes in dicyanoargenate (I) ions doped in alkali halide crystals. Exciplex tuning by site-selective excitation and variation of the dopant concentration. *Coord. Chem. Rev* **2000**, *208*, 227–241.

(2) Jansen, M. Homoatomic d10–d10 interactions: their effects on structure and chemical and physical properties. *Angew. Chem. Int. Ed.* **1987**, *26*, 1098–1110.

(3) Ford, P. C.; Vogler, A. Photochemical and photophysical properties of tetranuclear and hexanuclear clusters of metals with $d^10$ and $s^2$ electronic configurations. *Acc. Chem. Res.* **1993**, *26*, 220–226.

(4) Echavarren, A. M.; Jiao, N.; Gevorgyan, V. Coinage metals in organic synthesis. *Chem. Soc. Rev.* **2016**, *45*, 4445–4447.

(5) Horspool, W. M. *PATAI'S Chemistry of Functional Groups*; American Cancer Society, 2009.

(6) Echavarren, A. M.; Hashmi, A. S. K.; Toste, F. D. Gold Catalysis Steadily Increasing in Importance. *Adv. Synth. Catal.* **2016**, *358*, 1347–1347.

(7) Pflästerer, D.; Hashmi, A. S. K. Gold catalysis in total synthesis: recent achievements. *Chem. Soc. Rev.* **2016**, *45*, 1331–1367.

(8) Hashmi, A. S. K.; Hutchings, G. J. Gold Catalysis. *Angew. Chem. Int. Ed.* **2006**, *45*, 7896–7936.

(9) Huang, X.; El-Sayed, M. A. Gold nanoparticles: Optical properties and implementations in cancer diagnosis and photothermal therapy. *J. Adv. Res.* **2010**, *1*, 13 – 28.

(10) Barysz, M.; Pyykkö, P. Strong chemical bonds to gold. High level correlated relativistic results for diatomic $AuBe^+$, $AuC^+$, $AuMg^+$, and $AuSi^+$. *Chem. Phys. Lett.* **1998**, *285*, 398–403.

(11) Pyykko, P.; Riedel, S.; Patzschke, M. Triple-Bond Covalent Radii. *Chem. Eur. J.* **2005**, *11*, 3511–3520.

(12) Yu, M.; Bovet, N.; Satterley, C. J.; Bengio, S.; Lovelock, K. R.; Milligan, P.; Jones, R. G.; Woodruff, D.; Dhanak, V. True nature of an archetypal self-assembly system: Mobile Au-thiolate species on Au (111). *Phys. Rev. Lett.* **2006**, *97*, 166102.

(13) Grönbeck, H.; Häkkinen, H. Polymerization at the alkylthiolate-Au (111) interface. *J. Phys. Chem. B* **2007**, *111*, 3325–3327.

(14) Häkkinen, H.; Moseler, M.; Landman, U. Bonding in Cu, Ag, and Au Clusters: Relativistic Effects, Trends, and Surprises. *Phys. Rev. Lett.* **2002**, *89*, 033401.

(15) Nemcsok, D.; Wichmann, K.; Frenking, G. The significance of $\pi$ interactions in group 11 complexes with N-heterocyclic carbenes. *Organometallics* **2004**, *23*, 3640–3646.

(16) Marion, N.; Nolan, S. P. N-Heterocyclic carbenes in gold catalysis. *Chem. Soc. Rev.* **2008**, *37*, 1776–1782.

(17) Gorin, D. J.; Toste, F. D. Relativistic effects in homogeneous gold catalysis. *Nature* **2007**, *446*, 395–403.

(18) Salvi, N.; Belpassi, L.; Tarantelli, F. On the DewarâĂŞChattâĂŞDuncanson Model for Catalytic Gold(I) Complexes. *Chem. Eur. J.* **2010**, *16*, 7231–7240.

(19) Bistoni, G.; Belpassi, L.; Tarantelli, F. Disentanglement of Donation and Back-Donation Effects on Experimental Observables: A Case Study of Gold-Ethyne Complexes. *Angew. Chem. Int. Ed.* **2013**, *52*, 11599–11602.

(20) Ciancaleoni, G.; Biasiolo, L.; Bistoni, G.; Macchioni, A.; Tarantelli, F.; Zuccaccia, D.; Belpassi, L. Selectively Measuring $\pi$ Back-Donation in Gold (I) Complexes by NMR Spectroscopy. *Chem. Eur. J.* **2015**, *21*, 2467–2473.

(21) Dorel, R.; Echavarren, A. Gold(I)-Catalyzed Activation of Alkynes for the Construction of Molecular Complexity. *Chem. Rev.* **2015**, *115*.

(22) *Modern Gold Catalyzed Synthesis*; John Wiley & Sons, Ltd, 2012; pp 1–15.

(23) Grandinetti, F. *Noble Gas Chemistry: Structure, Bonding, and Gas-Phase Chemistry*; John Wiley & Sons, 2018.

(24) Pyykkö, P. Noblesse Oblige. *Science* **2000**, *290*, 64–65.

(25) Pan, S.; Jana, G.; Merino, G.; Chattaraj, P. K. Noble-Noble Strong Union: Gold at Its Best to Make a Bond with a Noble Gas Atom. *ChemistryOpen* **2019**, *8*, 173–187.

(26) Schröder, D.; Schwarz, H.; Hrusak, J.; Pyykkö, P. Cationic Gold(I) Complexes of Xenon and of Ligands Containing the Donor Atoms Oxygen, Nitrogen, Phosphorus, and Sulfur. *Inorg. Chem.* **1998**, *37*, 624–632.

(27) Seidel, S.; Seppelt, K. Xenon as a Complex Ligand: The Tetra Xenono Gold(II) Cation in AuXe42+(Sb2F11-)2. *Science* **2000**, *290*, 117–118.

(28) Cooke, S. A.; Gerry, M. C. L. XeAuF. *J. Am. Chem. Soc.* **2004**, *126*, 17000–17008.

(29) Belpassi, L.; Infante, I.; Tarantelli, F.; Visscher, L. The Chemical Bond between Au(I) and the Noble Gases. Comparative Study of NgAuF and $NgAu^+$ (Ng = Ar, Kr, Xe) by Density Functional and Coupled Cluster Methods. *J. Am. Chem. Soc.* **2008**, *130*, 1048–1060.

(30) Shayeghi, A.; Johnston, R. L.; Rayner, D. M.; Schäfer, R.; Fielicke, A. The Nature of Bonding between Argon and Mixed GoldâĂŞSilver Trimers. *Angew. Chem. Int. Ed.* **2015**, *54*, 10675–10680.

(31) Nunzi, F.; Cesario, D.; Pirani, F.; Belpassi, L.; Frenking, G.; Grandinetti, F.; Tarantelli, F. Helium Accepts Back-Donation In Highly Polar Complexes: New Insights into the Weak Chemical Bond. *J. Phys. Chem. Lett.* **2017**, *8*, 3334–3340, PMID: 28636399.

(32) Poggel, C.; Frenking, G. Relativistic Effects on Donor-Acceptor Interactions in Coinage Metal Carbonyl Complexes $[TM(CO)_n]^+$ (TM=Cu, Ag, Au; n=1, 2). *Chem. Eur. J.* **2018**, *24*, 11675–11682.

(33) Clark, L.; Lightfoot, P. Systems chemistry: All in a spin. *Nature Chem.* **2016**, *8*, 402–404.

(34) Kim, K. H. et al. Direct observation of bond formation in solution with femtosecond X-ray scattering. *Nature* **2015**, *518*, 385–389.

(35) Rawashdeh-Omary, M. A.; Omary, M. A.; Patterson, H. H.; Fackler, J. P. Excited-State Interactions for $[Au\ (CN)_2^-]_n$ and $[Ag\ (CN)_2^-]_n$ Oligomers in Solution. Formation of Luminescent Gold- Gold Bonded Excimers and Exciplexes. *J. Am. Chem. Soc.* **2001**, *123*, 11237–11247.

(36) Kim, K. H.; Kim, J. G.; Oang, K. Y.; Kim, T. W.; Ki, H.; Jo, J.; Kim, J.; Sato, T.; Nozawa, S.; ichi Adachi, S.; Ihee, H. Femtosecond X-ray solution scattering reveals that bond formation mechanism of a gold trimer complex is independent of excitation wavelength. *Structural Dynamics* **2016**, *3*, 043209.

(37) Iwamura, M.; Nozaki, K.; Takeuchi, S.; Tahara, T. Real-Time Observation of Tight Au–Au Bond Formation and Relevant Coherent Motion upon Photoexcitation of [Au (CN) 2–] Oligomers. *J. Am. Chem. Soc.* **2013**, *135*, 538–541.

(38) Wang, X.-B.; Wang, Y.-L.; Yang, J.; Xing, X.-P.; Li, J.; Wang, L.-S. Evidence of significant covalent bonding in $Au(CN)_2^-$. *J. Am. Chem. Soc.* **2009**, *131*, 16368–16370.

(39) Xiong, X.-G.; Wang, Y.-L.; Xu, C.-Q.; Qiu, Y.-H.; Wang, L.-S.; Li, J. On the gold–ligand covalency in linear [AuX 2]- complexes. *Dalton Trans.* **2015**, *44*, 5535–5546.

(40) Zaleski-Ejgierd, P.; Patzschke, M.; Pyykko, P. Structure and bonding of the MCN molecules, M= Cu, Ag, Au, Rg. *J. Chem. Phys.* **2008**, *128*, 224303–224303.

(41) Demissie, T. B.; Ruud, K. Darmstadtium, roentgenium, and copernicium form strong bonds with cyanide. *Int. J. Quantum Chem.* **2018**, *118*, e25393.

(42) Dietz, O.; Rayón, V. M.; Frenking, G. Molecular structures, bond energies, and bonding analysis of group 11 cyanides TM (CN) and isocyanides TM (NC)(TM= Cu, Ag, Au). *Inorg. Chem.* **2003**, *42*, 4977–4984.

(43) Wu, X.; Qin, Z.; Xie, H.; Cong, R.; Wu, X.; Tang, Z.; Fan, H. Photoelectron imaging and theoretical studies of group 11 cyanides MCN (M= Cu, Ag, Au). *J. Phys. Chem. A* **2010**, *114*, 12839–12844.

(44) Bistoni, G.; Belpassi, L.; Tarantelli, F. Advances in Charge Displacement Analysis. *J. Chem. Theory Comput.* **2016**, *12*, 1236–1244.

(45) Mitoraj, M. P.; Michalak, A.; Ziegler, T. A Combined Charge and Energy Decomposition Scheme for Bond Analysis. *J. Chem. Theory Comput.* **2009**, *5*, 962–975.

(46) Cappelletti, D.; Ronca, E.; Belpassi, L.; Tarantelli, F.; Pirani, F. Revealing Charge-Transfer Effects in Gas-Phase Water Chemistry. *Acc. Chem. Res.* **2012**, *45*, 1571–1580, PMID: 22775359.

(47) White, H. E. Pictorial Representation of the Dirac Electron Cloud for Hydrogen-Like Atoms. *Phys. Rev.* **1931**, *38*, 513.

(48) Bistoni, G.; Rampino, S.; Scafuri, N.; Ciancaleoni, G.; Zuccaccia, D.; Belpassi, L.; Tarantelli, F. How $\pi$ back-donation quantitatively controls the CO stretching response in classical and non-classical metal carbonyl complexes. *Chem. Sci.* **2016**, *7*, 1174–1184.

(49) Frenking, G. Chemical Bonding in Transition Metal Compounds. *The Chemical Bond* **2014**, 175–218.

(50) Orgel, L. 843. Stereochemistry of metals of the B sub-groups. Part I. Ions with filled d-electron shells. *J. Chem. Soc. (Resumed)* **1958**, 4186–4190.

(51) Jorgensen, C. K.; Pouradier, J. N 15.Un nouveau type de stabilisation du «champ des ligandes» dans les complexes linéaires du cuivre (I), de l'argent (I) et de l'or (I). *Journal de Chimie Physique* **1970**, *67*, 124–127.

(52) Sansonetti, J. E.; Martin, W. C. Handbook of Basic Atomic Spectroscopic Data. *J. Phys. Chem. Ref. Data* **2005**, *34*, 1559–2259.

(53) Schmidbaur, H. Supramolecular chemistry: Going for gold. *Nature* **2001**, *413*, 31.

(54) Bartocci, A.; Belpassi, L.; Cappelletti, D.; Falcinelli, S.; Grandinetti, F.; Tarantelli, F.; Pirani, F. Catching the role of anisotropic electronic distribution and charge transfer in halogen bonded complexes of noble gases. *J. Chem. Phys.* **2015**, *142*, 184304.

(55) Shannon, R. D. Revised effective ionic radii and systematic studies of interatomic distances in halides and chalcogenides. *Acta Cryst. A* **1976**, *32*, 751–767.

(56) Ball, P. Extreme chemistry: experiments at the edge of the periodic table. *Nature* **2019**, *565*, 552–555.

(57) Rampino, S.; Storchi, L.; Belpassi, L. Gold-superheavy-element interaction in diatomics and cluster adducts: A combined four-component Dirac-Kohn-Sham/charge-displacement study. *J. Chem. Phys.* **2015**, *143*, 024307.

(58) Salvi, N.; Belpassi, L.; Tarantelli, F. On the Dewar-Chatt-Duncanson Model for Catalytic Gold(I) Complexes. *Chem. Eur. J.* **2010**, *16*, 7231–7240.

(59) Zuccaccia, D.; Belpassi, L.; Macchioni, A.; Tarantelli, F. Ligand Effects on Bonding and Ion Pairing in Cationic Gold(I) Catalysts Bearing Unsaturated Hydrocarbons. *Eur. J. Inorg. Chem.* **2013**, *2013*, 4121–4135.

(60) Mitoraj, M.; Michalak, A. Natural orbitals for chemical valence as descriptors of chemical bonding in transition metal complexes. *J. Mol. Model.* **2007**, *13*, 347–355.

(61) Michalak Artur, Z. T., Mitoraj Mariusz Bond Orbitals from Chemical Valence Theory. *J. Phys. Chem. A* **2008**, *112*, 1933–1939.

(62) Bistoni, G.; Rampino, S.; Tarantelli, F.; Belpassi, L. Charge-displacement analysis via natural orbitals for chemical valence: Charge transfer effects in coordination chemistry. *J. Chem. Phys.* **2015**, *142*, 084112 (9).

(63) Nalewajski, R. F.; Mrozek, J. Modified valence indices from the two-particle density matrix. *Int. J. Quantum Chem.* **1994**, *51*, 187–200.

(64) Nalewajski, R. F.; Köster, A. M.; Jug, K. Chemical valence from the two-particle density matrix. *Theor. Chem. Acc.* **1993**, *85*, 463–484.

(65) Gaggioli, C. A.; Bistoni, G.; Ciancaleoni, G.; Tarantelli, F.; Belpassi, L.; Belanzoni, P. Modulating the Bonding Properties of N-Heterocyclic Carbenes (NHCs): A Systematic Charge-Displacement Analysis. *Chem. Eur. J.* **2017**, *23*, 7558–7569.

(66) Sorbelli, D.; Belpassi, L.; Tarantelli, F.; Belanzoni, P. Ligand Effect on Bonding in Gold(III) Carbonyl Complexes. *Inorg. Chem.* **2018**, *57*, 6161–6175, PMID: 29741374.

(67) De Santis, M.; Rampino, S.; Quiney, H. M.; Belpassi, L.; Storchi, L. Charge-Displacement Analysis via Natural Orbitals for Chemical Valence in the Four-Component Relativistic Framework. *J. Chem. Theory Comput.* **2018**, *14*, 1286–1296.

(68) Belpassi, L.; Storchi, L.; Quiney, H. M.; Tarantelli, F. Recent advances and perspectives in four-component Dirac-Kohn-Sham calculations. *Phys. Chem. Chem. Phys.* **2011**, *13*, 12368–12394.

(69) Grant, I. P.; Quiney, H. M. Application of relativistic theories and quantum electrodynamics to chemical problems. *Int. J. Quantum Chem.* **2000**, *80*, 283–297.

(70) Grant, I. P. *Relativistic quantum theory of atoms and molecules: theory and computation*; Springer series on atomic, optical, and plasma physics; Springer: Berlin, 2007.

(71) Storchi, L.; Rampino, S.; Belpassi, L.; Tarantelli, F.; Quiney, H. M. Efficient Parallel All-Electron Four-Component Dirac-Kohn-Sham Program Using a Distributed Matrix Approach II. *J. Chem. Theory Comput.* **2013**, *9*, 5356–5364.

(72) Rampino, S.; Belpassi, L.; Tarantelli, F.; Storchi, L. Full Parallel Implementation of an All-Electron Four-Component Dirac-Kohn-Sham program. *J. Chem. Theory Comput.* **2014**, *10*, 3766–3776.

(73) Dyall, K. G. Relativistic double-zeta, triple-zeta, and quadruple-zeta basis sets for the 5*d* elements Hf-Hg. *Theor. Chem. Acc.* **2004**, *112*, 403–409, Basis sets are available from the Dirac web site, http://dirac.chem.sdu.dk.

(74) Dyall, K. G.; Gomes, A. S. Revised relativistic basis sets for the 5*d* elements Hf-Hg. *Theor. Chem. Acc.* **2010**, *125*, 97–100, Basis sets are available from the Dirac web site, http://dirac.chem.sdu.dk.

(75) Dyall, K. Core correlating basis functions for elements 31-118. *Theor. Chem. Acc.* **2012**, *131*, 1–11, Basis sets are available from the Dirac web site, http://dirac.chem.sdu.dk.

(76) Dyall, K. G. Relativistic double-zeta, triple-zeta, and quadruple-zeta basis sets for the 4d elements Y–Cd. *Theor. Chem. Acc.* **2007**, *117*, 483–489.

(77) Dunning, T. H. Gaussian basis sets for use in correlated molecular calculations. I. The atoms boron through neon and hydrogen. *J. Chem. Phys.* **1989**, *90*, 1007–1023.

(78) Kendall, R. A.; Dunning Jr, T. H.; Harrison, R. J. Electron affinities of the first-row atoms revisited. Systematic basis sets and wave functions. *J. Chem. Phys.* **1992**, *96*, 6796–6806.

(79) Balabanov, N. B.; Peterson, K. A. Systematically convergent basis sets for transition metals. I. All-electron correlation consistent basis sets for the 3d elements Sc–Zn. *J. Chem. Phys.* **2005**, *123*, 064107.

(80) Schuchardt, K. L.; Didier, B. T.; Elsethagen, T.; Sun, L.; Gurumoorthi, V.; Chase, J.; Li, J.; Windus, T. L. Basis Set Exchange: A Community Database for Computational Sciences. *J. Chem. Inf. Model.* **2007**, *47*, 1045–1052, https://bse.pnl.gov/bse/portal.

(81) Grant, I. P.; Quiney, H. M. Rayleigh-Ritz approximation of the Dirac operator in atomic and molecular physics. *Phys. Rev. A* **2000**, *62*, 022508.

(82) Belpassi, L.; Tarantelli, F.; Sgamellotti, A.; Quiney, H. M. Electron density fitting for the Coulomb problem in relativistic density-functional theory. *J. Chem. Phys.* **2006**, *124*, 124104 (8).

(83) A. M. Köster, D. R. Salahub, et al., deMon2k, Version 4, The deMon developers. Cinvestav, Mexico City. 2016. `https://hadoop.apache.org`.

(84) De Santis, M.; Belapassi, L.; Tarantelli, F.; Storchi, L. Relativistic quantum chemistry involving heavy atoms. *Rendiconti Lincei. Scienze Fisiche e Naturali* **2018**, *29*, 209–217.

(85) Becke, A. D. Density-functional exchange-energy approximation with correct asymptotic behavior. *Phys. Rev. A* **1988**, *38*, 3098–3100.

(86) Lee, C.; Yang, W.; Parr, R. G. Development of the Colle-Salvetti correlation-energy formula into a functional of the electron density. *Phys. Rev. B* **1988**, *37*, 785–789.

(87) Breckenridge, W.; Ayles, V. L.; Wright, T. G. Evidence for Emergent Chemical Bonding in Au+- Rg Complexes (Rg= Ne, Ar, Kr, and Xe). *J. Phys. Chem. A* **2008**, *112*, 4209–4214.

(88) Baerends, E. J. et al. ADF2017, SCM, Theoretical Chemistry, Vrije Universiteit, Amsterdam, The Netherlands, https://www.scm.com.

# Graphical TOC Entry